Received: 7 July 2023 | Revised: 2 October 2023 | Accepted: 4 October 2023

DOI: 10.1002/pamm.202300255

RESEARCH ARTICLE

Towards realistic nonlinear elastic bending behavior for cable simulation

Tian Zhao[1,2] | **Fabio Schneider-Jung**[1] | **Joachim Linn**[1] | **Ralf Müller**[2]

[1]Department of Mathematics for Vehicle Engineering, Fraunhofer Institute for Industrial Mathematics ITWM, Kaiserslautern, Germany

[2]Department of Civil and Environmental Engineering, Technical University of Darmstadt, Darmstadt, Germany

Correspondence
Tian Zhao, Department of Mathematics for Vehicle Engineering, Fraunhofer Institute for Industrial Mathematics ITWM, Fraunhofer-Platz 1, 67663 Kaiserslautern, Germany.
Email: tian.zhao@itwm.fraunhofer.de

Funding information
Bundesministerium für Wirtschaft und Klimaschutz, Grant/Award Number: 19S21003C

Abstract

This contribution aims to characterize and model the nonlinear elastic behavior of cables for reliable simulations. To simulate the nonlinear elastic behavior of cables, we use an iterative method, where at each step, an algorithmic local bending stiffness constant is used and updated according to the current cable state. We also formulate an inverse problem to determine the properties of real cables. By solving the inverse problem, the nonlinear elastic behavior for given measurement data is identified, yielding a curvature-dependent bending stiffness characteristic. In addition, we propose an alternative method based on the balance equations for rods in static equilibrium to identify the bending stiffness characteristic. We apply both methods to experimental data, and the results are compared and discussed.

1 | INTRODUCTION

Flexible structures, such as cables and hoses, are widely used in the automotive industry [1]. The demand to reliably simulate such structures is, therefore, increased. Cosserat rod theory provides a suitable framework to model such flexible structures in a geometrically exact way. Linn et al. [2, 3] described a robust and efficient framework, in which the static equilibrium of the Cosserat rod is calculated by minimizing the potential energy. However, in these works, only linear elasticity was considered. For cables with more complex structures and materials, nonlinear elasticity plays an important role. We can observe such nonlinear elasticity in both pure bending tests [4] and MeSOMICS bending test [5]. In this work, we use a curvature-dependent bending stiffness characteristic to represent the nonlinear elastic bending behavior. To simulate such behavior, we presented an iterative method [6] based on the framework in Linn et al. [2]. In each iteration, the static equilibrium is calculated by minimizing the potential energy for linear elastic behavior, where an algorithmic local bending stiffness constant is included. The algorithmic local bending stiffness constant is updated according to a given curvature-dependent bending stiffness characteristic, and the iteration is repeated until the convergence of the cable state is achieved. Furthermore, we present two methods to determine the bending stiffness characteristics of real cables: an inverse problem and a method based on the equilibrium equations of the Cosserat rod. Since only quasi-static

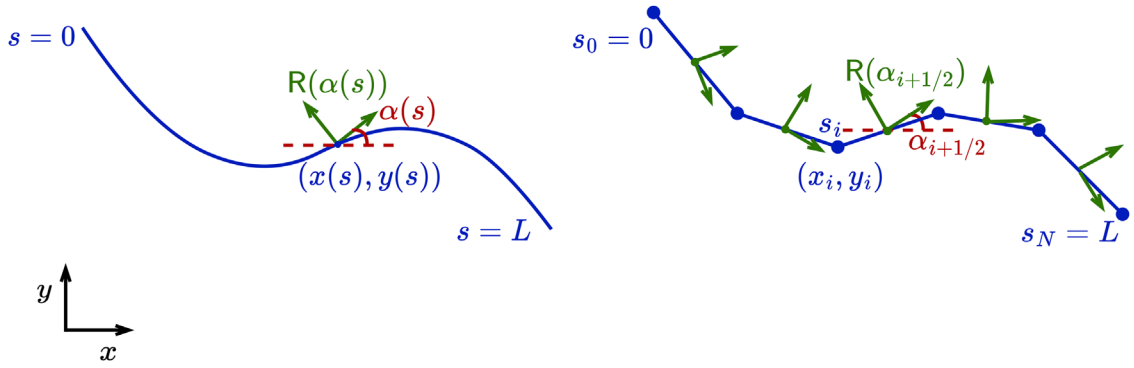

FIGURE 1 Left: Continuous Cosserat rod in $\mathbb{R}^2$. Right: Discrete Cosserat rod in $\mathbb{R}^2$.

experiments were considered to date, dynamic effects such as damping are not considered in the simulations presented in this work.

2 | COSSERAT ROD IN TWO-DIMENSIONAL SPACE

In this section, we show a brief introduction of the Cosserat rod in two-dimensional space, which was introduced in our previous works in Zhao et al. [6, 7].

The Cosserat rod in two-dimensional space (see Figure 1) consists of a centerline $(x(s), y(s))^T \in \mathbb{R}^2$ and the rotation angle $\alpha(s)$ parametrizing the local frame with rotation matrix

$$\mathsf{R}(s) = \begin{pmatrix} \cos(\alpha(s)) & -\sin(\alpha(s)) \\ \sin(\alpha(s)) & \cos(\alpha(s)) \end{pmatrix}, \tag{1}$$

where the curve parameter $s \in [0, L]$ is the arc length of the centerline in the reference configuration of the rod.

The curvature of the moving frame, which approximately corresponds to the curvature of the centerline, and the material tangent vector, which contains the components of the centerline tangent vector w.r.t the local frame, are given by

$$K(s) = \alpha'(s) \quad \text{and} \quad \boldsymbol{\Gamma}(s) = \begin{pmatrix} \Gamma_1(s) \\ \Gamma_2(s) \end{pmatrix} = \mathsf{R}(s)^T \begin{pmatrix} x(s) \\ y(s) \end{pmatrix}'. \tag{2}$$

The difference functions $\Delta K(s) = K(s) - \hat{K}_0(s)$ and $\Delta\boldsymbol{\Gamma}(s) = \boldsymbol{\Gamma}(s) - \boldsymbol{\Gamma}_0(s)$ represent the deviation of $K(s)$ and $\boldsymbol{\Gamma}(s)$ from the reference values $\hat{K}_0(s)$ and $\boldsymbol{\Gamma}_0 = (1, 0)^T$.

Following the work in Linn et al. [2], the static equilibrium state of the cables can be obtained by minimizing the potential energy

$$W = \frac{1}{2}\int_0^L \Delta\boldsymbol{\Gamma}^T(s)\mathsf{C}_{\boldsymbol{\Gamma}}\Delta\boldsymbol{\Gamma}(s)ds + \frac{1}{2}\int_0^L [EI]\Delta K(s)^2 ds, \tag{3}$$

where the first term represents the shear and tension energy, and the second term represents the bending energy. The effective tension stiffness $[EA]$ and effective shear stiffness $[GA]$ are assembled in the diagonal coefficient matrix $\mathsf{C}_{\boldsymbol{\Gamma}} = \mathrm{diag}([EA], [GA])$ and $[EI]$ is the effective bending stiffness.

The discrete potential energy can be written as

$$V = \frac{1}{2}\sum_{i=0}^{N-1} \Delta s_{i+1/2}(\Delta\boldsymbol{\Gamma}_{i+1/2})^T\mathsf{C}_{\boldsymbol{\Gamma}}\Delta\boldsymbol{\Gamma}_{i+1/2} + \frac{1}{2}\sum_{i=0}^{N} \delta s_i[EI]\Delta K_i^2, \tag{4}$$

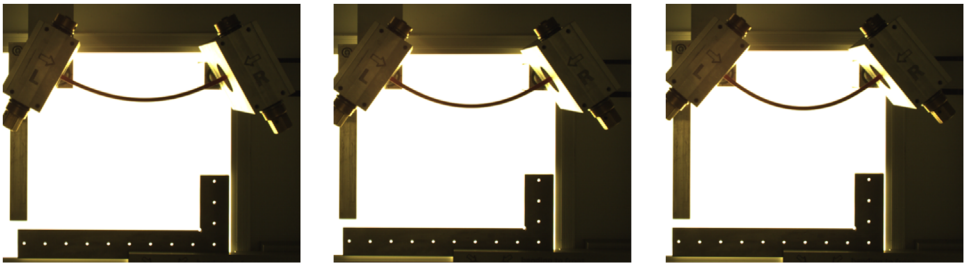

FIGURE 2 Top-view of real bending experiment on cable 1. Left: Cable configuration (a), with applied displacement d. Middle: Cable configuration (b), with applied displacement $2d$. Right: Cable configuration (c), with applied displacement $3d$.

where the index i denotes vertex quantities at s_i for $i = 0, \dots, N$ and $i + 1/2$ denotes edge-centered quantities at $s_{i+1/2}$ for $i = 0, \dots, N - 1$. More details about the derivation from the continuous case can be found in Linn et al. [2].

3 | BENDING EXPERIMENTS

Real and virtual bending experiments are performed to study the bending behavior of cables.

The real experiments are performed on the MeSOMICS measurement machine [5]. As shown in Figure 2, the specimen is clamped at both ends. Both clamping devices are inserted in (approximately) moment-free bearings. The left clamping point is stepwise shifted towards the right clamping point, resulting in corresponding bending deformations. By moving back to the start point, one bending cycle is achieved. Such cycle repeats five times, and here, we evaluate the fourth cycle. Meanwhile, the resulting reaction force is measured at the right clamping point. For each configuration, the bending deformations are recorded by a camera and the corresponding cable centerline is detected. Figure 2 shows the captured bending deformation of a cable specimen (cable 1) with length $L = 181$ mm and diameter $d = 4.6$ mm (cross section as shown in the left picture of Figure 3). The three images in Figure 2 show cable configurations (a), (b), and (c) with applied displacements of d, $2d$, and $3d$, respectively. Furthermore, we perform the bending experiment on a high-voltage cable specimen (cable 2), which has a length of 226 mm and a diameter of 17.4 mm, the cross section is as shown in the right picture of Figure 3.

We also perform virtual bending experiments in a two-dimensional space by using the Cosserat rod model from Section 2. The boundary conditions of the virtual experiment are the same as those for the real experiment. In the virtual experiment, both ends are moment-free. By applying displacements to one end, the resultant forces on the other end are computed.

4 | SIMULATING NONLINEAR ELASTIC BEHAVIOR

To represent the nonlinear elastic bending behavior, we introduce a curvature-dependent bending stiffness characteristic $f_{EI}(\kappa)$. With that, the bending energy term is written as

$$V_{B,nl} = \sum_{i=0}^{N} \delta s_i \int_{\hat{K}_{0,i}}^{K_i} \int_{\hat{K}_{0,i}}^{\xi} f_{EI}(\kappa) d\kappa d\xi. \tag{5}$$

FIGURE 3 Left: Cross section of cable 1. Right: Cross section of cable 2.

TABLE 1 Model parameters for virtual bending experiment.

Parameter	L	$\hat{\kappa}_0$	$\hat{\kappa}_1$	$\hat{\kappa}_2$	$[\hat{EI}]_0$	$[\hat{EI}]_1$	$[\hat{EI}]_2$	$\hat{K}_{0,i}$	N	$[EA]$	$[GA]$
Unit	[m]	[m^{-1}]	[m^{-1}]	[m^{-1}]	[Nm^2]	[Nm^2]	[Nm^2]	[m^{-1}]	–	[N]	[N]
Value	0.2	0	5	10	$1 \cdot 10^{-3}$	$3 \cdot 10^{-3}$	$3.5 \cdot 10^{-3}$	0	11	1000	1000

Using $V_{B,nl}$ as bending energy term, the energy minimization problem could be solved directly. However, this requires expensive computations. To use the curvature-dependent bending stiffness characteristic with Cosserat rod in two-dimensional space (as described in Section 2) while maintaining its efficiency, we use an iterative method. In each step, we still consider linear elasticity and solve the static equilibrium by energy minimization. More precisely, an algorithmic local bending stiffness constant is applied here. In the mth iteration step, a given cable state (x_i^m, y_i^m), $i = 0, \dots, N$ and $\alpha_{i+1/2}^m$, $i = 0, \dots, N-1$ yields corresponding curvatures K_i^m. The algorithmic local bending stiffness constant is updated according to the given bending stiffness characteristic and the curvatures K_i^m. Then minimizing the potential energy leads to a new equilibrium state (x_i^{m+1}, y_i^{m+1}), $\alpha_{i+1/2}^{m+1}$ and corresponding curvatures K_i^{m+1}. This process is repeated until the cable state converges, that is, $\sum_{i=0}^{N} \delta s_i \cdot |K_i^m - K_i^{m+1}| < tol$ is fulfilled. More technical details regarding the iterative method can be found in Zhao et al. [6].

We perform virtual bending experiments to demonstrate the iterative method. Here, the curvature-dependent bending stiffness characteristic is parametrized using a natural cubic spline with three control points, denoted by $(\hat{\kappa}_0, [\hat{EI}]_0)$, $(\hat{\kappa}_1, [\hat{EI}]_1)$ and $(\hat{\kappa}_2, [\hat{EI}]_2)$. We also perform a virtual bending experiment with a direct solution for the bending energy term in Equation (5) as reference solution to validate the iterative method. The model parameters are listed in Table 1.

The plots in Figure 4 show the discrete curvature K_i over the arc length s_i for the cable states in the single iteration steps, while the boundary conditions are unchanged. One can observe that after six iterations, the curvature in the iterative method converges to the curvature values of the reference solution (illustrated by the black dashed line). Figure 5 plots the horizontal reaction force virtually measured at the fixed end point for a sequence of applied displacements. A very good agreement is observed between the horizontal reaction force simulated by iterative method and the reference solution.

Moreover, the iterative method is computationally more efficient (in this example, approximately five times faster) than directly solving the energy minimization problem with Equation (5).

5 | IDENTIFICATION OF NONLINEAR ELASTIC BEHAVIOR

Above, we discussed how to utilize a bending stiffness characteristic, that is, nonlinear elastic behavior, in our cable simulation. Now, our focus shifts to determining the bending stiffness characteristic from given measurement results.

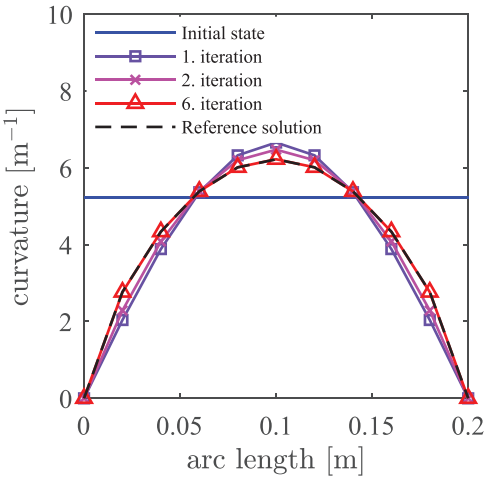

FIGURE 4 Discrete curvatures in each iteration.

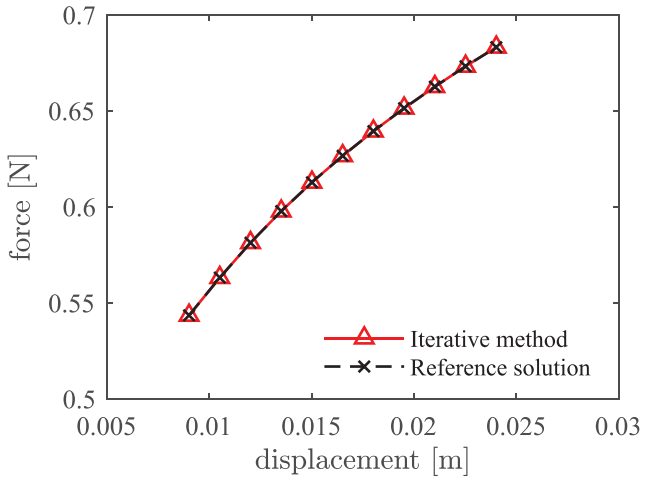

FIGURE 5 Horizontal reaction force obtained at the fixed end point, resulting from varying displacements.

5.1 | Inverse problem

To determine the bending stiffness characteristic, we formulate an inverse problem (see Zhao et al. [6, 7]). Our objective is to determine a bending stiffness characteristic that allows the simulated horizontal reaction force and curvature of the cable to closely align with the actual measured force and the cable curvature obtained from the bending tests.

As described in Section 4, the curvature-dependent bending stiffness characteristic is parametrized by a natural cubic spline with three control points. For simplicity, we assume that $\hat{\kappa}_0$, $\hat{\kappa}_1$, and $\hat{\kappa}_2$ are fixed, and consider only $[\hat{EI}]_0$, $[\hat{EI}]_1$, and $[\hat{EI}]_2$ as optimization variables. Furthermore, we take into account the influence of the precurvature $\hat{K}_0(s)$ by including it as an optimization variable. This is necessary, because on one hand, the cable specimen under investigation is not perfectly straight in the absence of applied loading, but instead slightly bent. On the other hand, the precurvature can also approximate the impact of the plastic curvature due to (cyclic) bending. This additional plastic curvature only occurs in regions of strong bending curvature. So in general, the precurvature $\hat{K}_0(s)$ can explicitly depend on the arc length s and vary along the cable. However, in this work, we consider the precurvature as constant, denoted as $\hat{K}_0$. Using such a precurvature $\hat{K}_0(s)$ as an optimization variable can capture the plastic effect to a certain extent, albeit in a rough approximation. The optimization is performed using a Levenberg–Marquardt method in MATLAB [8].

We apply the real bending experiment data to the inverse problem and aim to find the characteristic $f_{EI}(\kappa)$ for a real cable. The bending experiment and the cable used in test is detailed in Section 3.

The identified bending stiffness characteristic for cable 1 is shown in Figure 6. The blue dashed line represents the solution of the inverse problem without consideration of the precurvature, that is, with a priori defined precurvature $\hat{K}_0 = 0$.

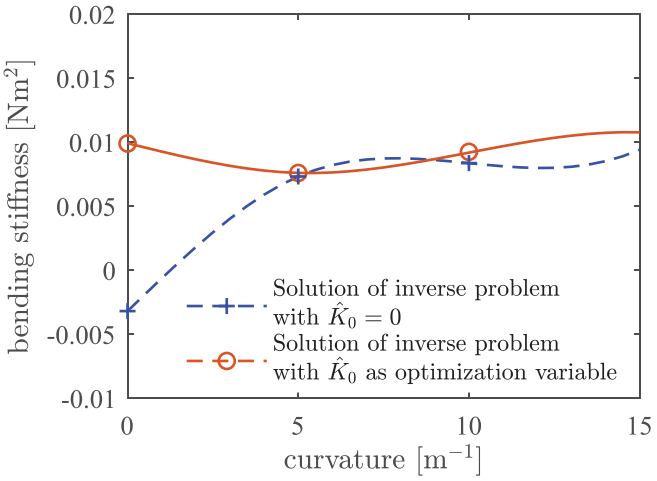

FIGURE 6 Identified bending stiffness characteristic (with set $\hat{K}_0 = 0$ and $\hat{K}_0$ as optimization variable) for cable 1.

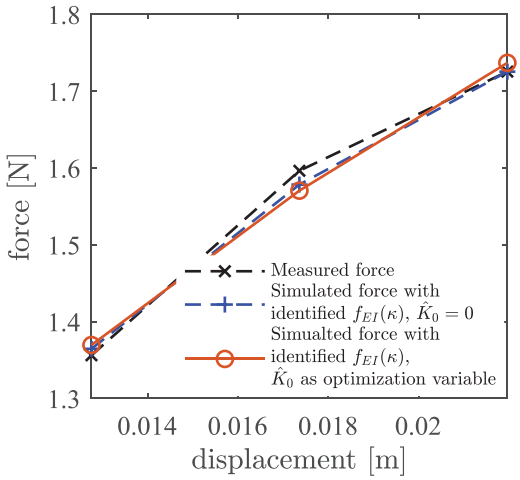

FIGURE 7 Measured and simulated force for cable 1 (blue: with dashed blue characteristic and $\hat{K}_0 = 0$; orange: with solid orange characteristic and identified $\hat{K}_0$).

The solid orange line shows the solution of the inverse problem obtained when the precurvature is considered as an optimization variable (identified precurvature $\hat{K}_0 \approx 3.1\,\mathrm{m}^{-1}$). Looking at the corresponding simulated forces in Figure 7 (orange and blue dashed lines), both characteristics lead to good matches with the measured forces (black dashed line). However, comparing the two identified characteristics (see Figure 6), the solution without consideration of the precurvature exhibits negative values for low curvatures, while considering the precurvature as an optimization leads to a more realistic bending stiffness characteristic. This indicates that it is important to include precurvature in the optimization. Furthermore, the solution of the inverse problem with consideration of precurvature (see Figure 6) shows an almost constant bending stiffness, which is plausible due to the simple structure of this cable.

Furthermore, we evaluated the cable 2, which has a more complex structure. The identified bending stiffness characteristic is shown in Figure 8 (identified precurvature $\approx 3.9\,\mathrm{m}^{-1}$). It is clear that for this cable, the bending stiffness varies with its curvature. Moreover, as shown in Figure 9, the simulated force using the identified characteristic and the precurvature is in good agreement with the measured value.

Overall, when applied to experimental data, solving the inverse problem yields physically plausible bending stiffness characteristics.

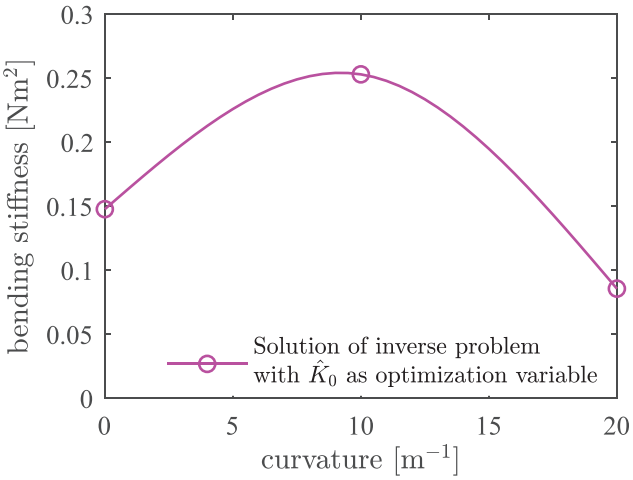

FIGURE 8 Identified bending stiffness characteristic for cable 2.

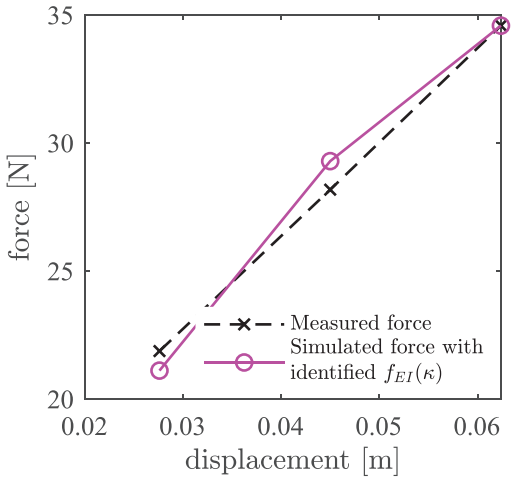

FIGURE 9 Measured and simulated force for cable 2.

5.2 | Balance equations and $(\kappa, f_{EI}(\kappa))$-graph

In order to evaluate the bending stiffness characteristic determined as a solution of the inverse problem, we introduced an alternative approach in Zhao et al. [7], which is based on the balance equations for a Cosserat rod.

First, we summarize such a observables-based method as described in Zhao et al. [7].

In the absence of external body forces and moments acting on the Cosserat rod, the equilibrium equations are given by

$$\partial_s \mathbf{f} = \mathbf{0}, \tag{6}$$

$$\partial_s \mathbf{m} + \partial_s \boldsymbol{\varphi} \times \mathbf{f}(s) = \mathbf{0}, \tag{7}$$

where $\boldsymbol{\varphi}(s) = (x(s), y(s), z(s))^T \in \mathbb{R}^3$ is the centerline of the rod, $\mathbf{f}(s) = (f^x(s), f^y(s), f^z(s))^T \in \mathbb{R}^3$ is the force vector, and $\mathbf{m}(s) = (m^x(s), m^y(s), m^z(s))^T \in \mathbb{R}^3$ is the moment vector. Equations (6) and (7) hold independent of the constitutive behavior of the rod [9].

Integrating Equations (6) and (7) leads to

$$\mathbf{f}(s) = \mathbf{f}, \tag{8}$$

$$\partial_s \mathbf{m} + \partial_s \boldsymbol{\varphi} \times \mathbf{f}(s) = \mathbf{0}, \tag{9}$$

here $\mathbf{f}$ and $\boldsymbol{\mathcal{M}}$ are constant along the rod.

In two-dimensional space, for the rod in the x–y plane (see Figure 1), it holds $\boldsymbol{\varphi}(s) = (x(s), y(s), 0)^T$, $\mathbf{f}(s) = (f^x(s), f^y(s), 0)^T$, and $\mathbf{m}(s) = (0, 0, m(s))^T$. Thus, Equation (9) can be written as

$$m(s) + x(s) f^y - y(s) f^x = \mathcal{M}, \tag{10}$$

where $\mathcal{M}$ is a constant scalar.

For our bending experiment (see Figure 2), at both simply supported end points, the bending moment fulfills $m(0) = 0$ and $m(L) = 0$. Since the relative displacement of the boundary conditions is applied along the x-axis and both ends are moment-free, the reaction force in y-direction vanishes, that is, $f^y = 0$. Moreover, we choose the origin, such that $\mathcal{M} = 0$, that is, such that $y(0) = 0$. Thus, Equation (10) simplifies to $m(s) = y(s) f^x$, which represents the bending moment at arc length s.

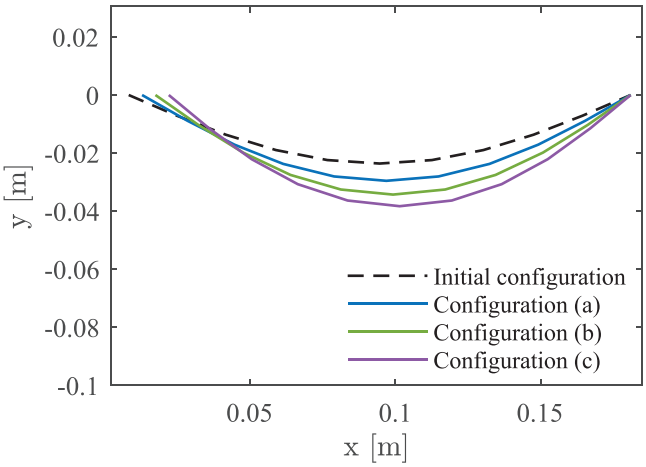

FIGURE 10 Simulated bending configurations (a), (b), and (c).

When $[EA]$ and $[GA]$ are relatively large (see Table 1), the Cosserat model can be approximated as an inextensible Kirchhoff model. Therefore, the curvature of the bending line can be further calculated using $K(s) = \frac{d\theta(s)}{ds}$, where $\theta(s) = \arctan(\frac{dy}{dx})$. The state-dependent bending stiffness for curvature $K(s)$ can be obtained by $\frac{dm(\kappa)}{d\kappa}|_{\kappa=K(s)} =: f_{EI}(K(s))$.

Therefore, given the measured horizontal reaction force and the optically detected bending line, we can determine the bending stiffness $f_{EI}(K(s))$ at curvature $K(s)$. Since our bending experiment results in a range of curvatures in the rod, we obtain a $(K(s), f_{EI}(K(s)))$-graph for each configuration.

The experimental data of cable 1, which are applied to the inverse problem, are further used to generate $(\kappa, f_{EI}(\kappa))$-graphs.

Figure 10 displays the $(K(s), f_{EI}(K(s)))$-graphs for configurations (a), (b), and (c) (see Figure 11), which correspond to the pictures in Figure 2. We observe good consistency among the three identified graphs, indicating the potential to combined them into one single bending stiffness characteristic. However, when comparing the results with those from the inverse problem (the red line in Figure 10), we observe clear deviations. While the order of magnitude is similar, there are clear qualitative discrepancies. Investigating the source of such discrepancies is a topic of our current research.

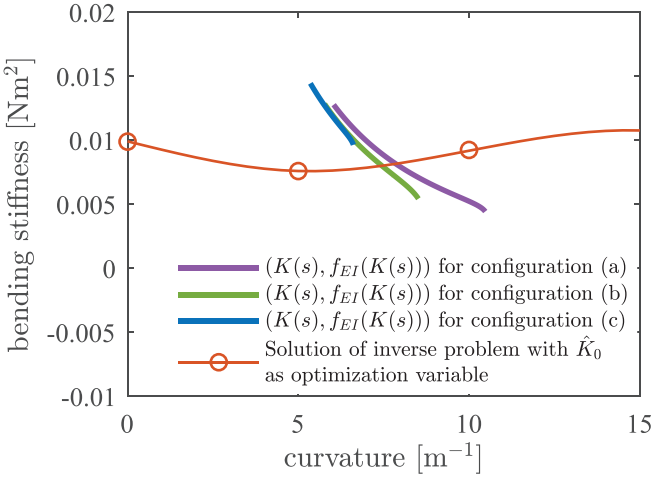

FIGURE 11 $(K(s), f_{EI}(K(s)))$-graphs determined by method based on balance equations, together with the $f_{EI}(\kappa)$ identified via the inverse problem.

6 | SUMMARY AND OUTLOOK

In this work, we presented two aspects related to investigating the simulation of nonlinear elastic behavior in cables. First, the iterative method demonstrates that we can correctly and efficiently simulate the nonlinear elastic behavior. Additionally, the corresponding inverse problem allows us to access the experimentally observed nonlinear elastic behavior of cables. The identified characteristic including the influence of the precurvature yields physical plausible results. The observables-based method offers the potential to directly identify the bending stiffness characteristic from the optically detected bending line and measured reaction force. Nevertheless, there are discrepancies between the results from the inverse problem and the observables-based $(K(s), f_{EI}(K(s)))$-graphs, the further comparison of these results remains of interest. Our next step is to understand the source of such discrepancies.

ACKNOWLEDGMENTS

This work is part of the "BordNetzSim3D"-project (funding code: 19S21003C), funded by the German Federal Ministry for Economic Affairs and Climate Action.

Open access funding enabled and organized by Projekt DEAL.

ORCID

Tian Zhao https://orcid.org/0009-0004-3874-2349

REFERENCES

1. Linn, J., Schneider, F., Dreßler, K., & Hermanns, O. (2022). In H. G. Bock, K. H. Küfer, P. Maass, A. Milde, & V. Schulz (Eds.), Virtual product development and digital validation in automotive industry. *Mathematics in industry* (Vol. 35). Springer.
2. Linn, J., Hermansson, T., Andersson, F., & Schneider, F. (2017). Kinetic aspects of discrete cosserat rods based on the difference geometry of framed curves. *Proceedings of the ECCOMAS Thematic Conference on Multibody Dynamics, Prague, Czech Republic*, 163–176.
3. Linn, J., Stephan, T., Carlsson, J., & Bohlin, R. (2008). In L. L. Bonilla, M. Moscoso, G. Platero, & J. M. Vega (Eds.), Fast simulation of quasistatic rod deformations for VR applications. *Progress in industrial mathematics at ECMI 2006*. Mathematics in industry (Vol. 12). Springer.
4. Dörlich, V., Linn, J., & Diebels, S. (2018). In H. Altenbach, F. Jablonski, W. Müller, K. Naumenko, & P. Schneider (Eds.), Flexible beam-like structures - experimental investigation and modeling of cables. *Advances in mechanics of materials and structural analysis*. Advanced structured materials (Vol. 80, pp. 27–46). Springer.
5. *MeSOMICS: Measurement system for the optically monitored identification of cable stiffnesses.* http://www.mesomics.eu
6. Zhao, T., Schneider-Jung, F., Linn, J., & Müller, R. (2022). Simulating nonlinear elastic behaviour of cables using an iterative method. *European congress on computational methods in applied sciences and engineering*, Oslo, Norway.
7. Zhao, T., Schneider-Jung, F., Linn, J., & Müller, R. (2023). Identification of nonlinear elastic bending behavior for cable simulation. *ECCOMAS thematic conference on multibody dynamics*, Lisbon, Portugal.
8. The MathWorks Inc. *Natick, Massachusetts, United States.* https://www.mathworks.com
9. Simo, J. C. (1985). A finite strain beam formulation. The three-dimensional dynamic problem. Part I. *Computer Methods in Applied Mechanics and Engineering*, *49*, 55–70.

How to cite this article: Zhao, T., Schneider-Jung, F., Linn, J., & Müller, R. (2023). Towards realistic nonlinear elastic bending behavior for cable simulation. *Proceedings in Applied Mathematics and Mechanics*, *23,* e202300255. https://doi.org/10.1002/pamm.202300255